The SHURUI System: A Modular Continuum Surgical Robotic Platform for Multiport, Hybrid-Port, and Single-Port Procedures

Yuyang Chen, Chao Zhang, Zhonghao Wu, *Student Member, IEEE*, Jiangran Zhao, Bo Yang, Jia Huang, Qingquan Luo, Linhui Wang, and Kai Xu, *Member, IEEE*

***Abstract*—In the past decades, numerous surgical robotic systems have been developed to improve dexterity, precision, and ergonomics in minimally invasive surgery (MIS). These robotic systems usually have different forms to accommodate the requirements from either multiport or single-port procedures. Unlike the design consensus in the multiport systems where distal-wristed and straight-stemmed instruments are maneuvered by patient-side manipulators, different approaches are still being explored to verify the fulfillment of the clinical and functional requirements from single-port procedures. No systems have been shown to satisfactorily handle both the multiport and the single-port procedures. Utilizing the previously proposed dual continuum mechanism to realize a payload-enhanced multidegree of freedom surgical instrument with a tight bending wrist for intra-abdomen dexterity, it was found that the locations and the number of channels of the access ports can be freely configured. A modular surgical robotic platform is, hence, proposed for handling multiport, single-port, and for the first time hybrid-port procedures. The design concepts, system descriptions, teleoperation kinematics, experimental characterizations, and animal studies are reported. It is expected that *suitable invasiveness*, where a minimal number of skin incisions can always be used to treat a condition, is to be achieved by the proposed system. True potentials of the proposed system are to be verified in the coming larger scale animal studies and clinical trials.**

***Index Terms*—Dual continuum mechanism, hybrid-port procedure, multiport procedure, single-port procedure, surgical robotic platform.**

I. Introduction

MANIPULATION challenges in laparoscopic and thoracoscopic minimally invasive surgery (MIS) have stimulated the development of surgical robotic systems in the past three decades [1]–[3]. Robotic technologies have improved motion precision, distal dexterity, visual guidance, and surgeon ergonomics for enhanced patient benefits, such as shortened hospital stay, reduced complications, and improved cosmesis. For multiport procedures, surgical instruments are deployed into a patient's abdomen through multiple skin incisions. Numerous existing designs converged to a design consensus: multiple distal-wristed and straight-stemmed surgical instruments are maneuvered by several extracorporeal manipulators through the skin incisions. The distal wrists for dexterity enhancement can be designed using different approaches, such as cable actuation [4], serial linkage actuation [5], parallel linkage [6], continuum segments [7], [8], and deformable structures [9]. On the other hand, the extracorporeal manipulators shall realize remote-center-of-motion (RCM) movements to satisfy the constraints imposed by the skin incisions. The RCM movements can be realized by kinematically constrained mechanisms (e.g., the parallelograms and their equivalents [4], [10], [11], serial spherical linkage [12], goniometer arcs [7]), passive RCM mechanisms [13], and programmed joints movements coordination [8], [14], [15].

In order to further reduce the invasiveness of the multiport MIS, single-port surgery was introduced [16]. Single-port surgery demonstrated its safety and effectiveness comparable to the multiport surgery in general surgery, gynecologic surgery, urologic surgery, and thoracic surgery, with reduced postoperative pain and improved cosmetic outcomes.

Due to the manipulation difficulties in the single-port procedures, many surgical robots have been developed. Unlike the design consensus for the multiport surgical platforms, different

Manuscript received March 18, 2021; revised July 8, 2021; accepted August 15, 2021. Recommended by Technical Editor J.-H. Han and Senior Editor G. Alici. This work was supported in part by the National Key R&D Program of China under Grant 2019YFC0118003, Grant 2017YFC0110800, and Grant 2019YFC0118004, in part by the Science and Technology Commission of Shanghai Municipality under Grant 20DZ2220400, and in part by the National Natural Science Foundation of China under Grant 51722507. *(Corresponding author: Kai Xu.)*

Yuyang Chen and Zhonghao Wu are with the Laboratory of Robotics Innovation and Intervention, UM-SJTU Joint Institute, Shanghai Jiao Tong University, Shanghai 200240, China (e-mail: supandoria@sjtu.edu.cn; zhonghao.wu@sjtu.edu.cn).

Chao Zhang, Bo Yang, and Linhui Wang are with the Department of Urology, Shanghai Changhai Hospital, Naval Medical University, Shanghai 200433, China (e-mail: tony373@163.com; yangbochanghai@126.com; wanglinhuicz@163.com).

Jiangran Zhao is with the Beijing Surgerii Technology Company, Ltd., Beijing 100192, China (e-mail: jiangran.zhao@surgerii.com).

Jia Huang and Qingquan Luo are with the Shanghai Lung Cancer Center, Shanghai Chest Hospital, Shanghai Jiao Tong University, Shanghai 200030, China (e-mail: huangjiadragon@126.com; luoqingquan@hotmail.com).

Kai Xu is with the School of Mechanical Engineering, Shanghai Jiao Tong University, Shanghai 200240, China (e-mail: k.xu@sjtu.edu.cn).

This article has supplementary material provided by the authors and color versions of one or more figures available at https://doi.org/10.1109/TMECH.2021.3110883.

Digital Object Identifier 10.1109/TMECH.2021.3110883

approaches are still being explored to verify whether the clinical and functional requirements have been fulfilled.

The patient-side manipulators of a single-port surgical platform can either adopt an "X" configuration or a "Y" configuration. In the "X" configuration, all instruments are inserted into a patient's abdomen in a crossed manner (e.g., in [17] and [18]). Particular attentions shall be directed to instrument collision avoidance. In a "Y" configuration, the instruments are inserted in a parallel manner through a multichannel sheath. Different actuation schemes have been devised, including the cable-driven articulation (e.g., the da Vinci SP system [19] and the SPORT system [20]), embedded motors [21], [22], spatial linkages [23], and continuum mechanisms [24], [25]. The primary challenge of the "Y" configuration lies on the conflicting demands for large workspace and adequate payload capability of the surgical tools.

Single-port surgery may offer an effective, safe alternative to multiport procedures with less invasiveness. But multiport surgery has been more widely adopted as standard of care. The multiport paradigm might be more suitable for multiquadrant procedures. The use of a multiport or a single-port treatment may be, in theory, preferred towards different patient groups [26], [27]. But multiport or single-port procedures may have to be conducted by different surgical robotic systems, since most existing surgical robotic platforms are designed aiming at either multiport or single-port paradigm. Few systems are shown to handle both single-port and multiport surgeries, except the da Vinci VeSPA [28] single-site instruments kit that can be installed on a da Vinci Si system. But only the VeSPA single-site needle driver has a distal wrist with reduced joint ranges, compared to a standard EndoWrist. The VeSPA kit usage does not prevail, possibly due to the reduced dexterity.

Using the previously proposed dual continuum mechanism [25], it was found that the access ports for the multidegree of freedom (DoF) surgical instrument can be freely configured, while maintaining the instrument's payload capability and intra-abdomen dexterity. This article, hence, proposes a modular surgical robotic platform, the SHURUI system, for multiport, single-port, and for the first time, hybrid-port procedures, where the skin incision locations and the number of channels of the access ports can be freely configured.

As shown in Fig. 1, the SHURUI system consists of a surgeon console, an equipment cart and several identical patient-side carts. An endoscopic tool or a surgical tool can be equipped to any of the patient-side carts. In the preoperative stage, a desired system configuration (a.k.a. the multiport, the single-port, or the hybrid-port paradigm), is decided according to a patient's condition. The patient-side carts are then set up around the surgical bed according to the desired configuration. This patient-side cart configuration is usually kept until the procedure is completed. The proposed platform thus potentially permits *suitable invasiveness*, where a minimum number of skin incisions can be commanded by a surgeon to treat different pathological conditions for improving surgical outcomes.

The main contributions of this article are summarized as follows. First, a unified teleoperation framework is introduced for arbitrary trocar arrangement to realize multiport, single-port, and hybrid-port surgery. Second, a modular system configuration of the SHURUI system with the individual patient-side cart design is proposed to accommodate the aforementioned procedures. Third, with the design embodiment towards the actual clinical requirements, this article truly shows the feasibility of continuum surgical robots towards actual laparoscopic and thoracoscopic surgeries.

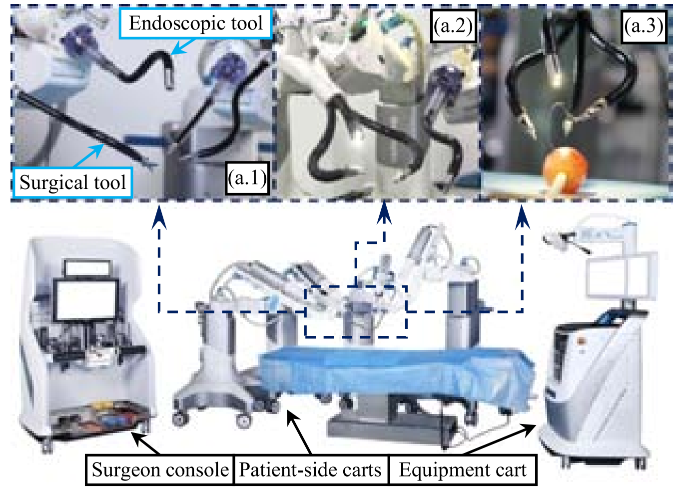

Fig. 1. Overview of the SHURUI system. The patient-side carts can be arranged to deploy the surgical/endoscopic tools in the (a.1) multiport, (a.2) hybrid-port, and (a.3) single-port configurations.

The rest of this article is organized as follows. In Section II, the key design concepts of the surgical platform are introduced, while the platform descriptions are presented in Section III. In Section IV, the kinematics framework for tool control and teleoperation is elaborated. The experimental characterizations and validations, including animal studies, are reported in Section V. Finally, Section VI concludes this article.

II. Design Concepts

A key design objective of the SHURUI system is to cover different surgical paradigms, e.g., the multiport, hybrid-port, and single-port procedures. This goal has to be achieved, essentially by realizing the movements of surgical end-effectors with enough translational and orientation ranges and adequate payload capability, even via different access ports.

This design objective has not been accomplished by the technical approaches used in the existing robotic surgical systems mentioned in Section I. These existing systems either adopt i) straight-stemmed or curved-stemmed instruments (e.g., the da Vinci EndoWrist instruments or the VeSPA Single-Site instruments), or ii) multi-DoF articulated instruments (e.g., the ones actuated by cables, embedded motors, or spatial linkages).

When a multi-DoF articulated instrument is used in a single-port surgical robot with a "Y" configuration, such an instrument is subject to a poor loading condition for its shoulder joint. In Fig. 2(a.2), the external load has a long moment arm. For cable-driven instruments, such a condition leads to a high tension in the pulling cable, and resultantly a low joint stiffness due to the non-negligible cable elongations.

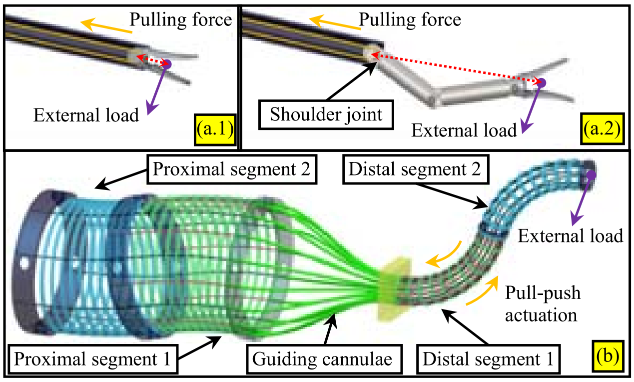

Fig. 2. Different loading conditions for (a.1) a cable-driven wristed tool, (a.2) a cable-driven articulated instrument, and (b) a dual continuum mechanism.

On the contrary, a wrist joint in a rigid-stemmed tool is subject to a much shorter moment arm, as shown in Fig. 2(a.1). Hence using pulling cables well actuates the distal wrists.

A key enabler for the proposed modular continuum surgical robotic platform is the dual continuum mechanism [25] with enhanced payload capability. As shown in Fig. 2(b), bending of a proximal segment is coupled to that of the distal segment via pulling and pushing of all the redundantly arranged structural backbones. Then, the external load is balanced collaboratively by the pull–push actuation of all these redundant backbones. What's more, thin backbones can be used for the distal segment 2 to realize a tight bending for intra-abdomen dexterity. The segment's payload capability will not be comprised because the number of the backbones is increased.

Using the dual continuum mechanism to design continuum instruments with adequate dexterity and payload capability, it was found that the locations and the number of the skin incisions can be arbitrarily determined for multiport, hybrid-port, and single-port procedures. Then, designs of the SHURUI system, including the system layout, the patient-side carts, the surgical tools, the endoscopic tool, the accessories, etc., converge to their final forms, as shown in Figs. 1 and 3.

Different patient-side configurations of the SHURUI system for the multiport, hybrid-port, and single-port procedures are presented in Fig. 3.

In the multiport configuration, the tools are inserted into the abdomen via standard trocars. The patient-side carts are individually parked near the insertion port to facilitate the tools' deployment. Since the continuum surgical tools possess six DoFs for intracorporeal movements, extracorporeal RCM movements are not necessary. Only a lockable stand is integrated into the patient-side cart for positioning and orienting of the surgical/endoscopic tools.

In the hybrid-port procedure, two skin incisions are made for a standard trocar and a customized three-channel trocar. While one surgical tool is deployed via the standard trocar, one endoscopic tool and two surgical tools are inserted through the three-channel trocar.

In both the multiport and the hybrid-port configurations, the relative tool motions depend on the trocar geometry as well as

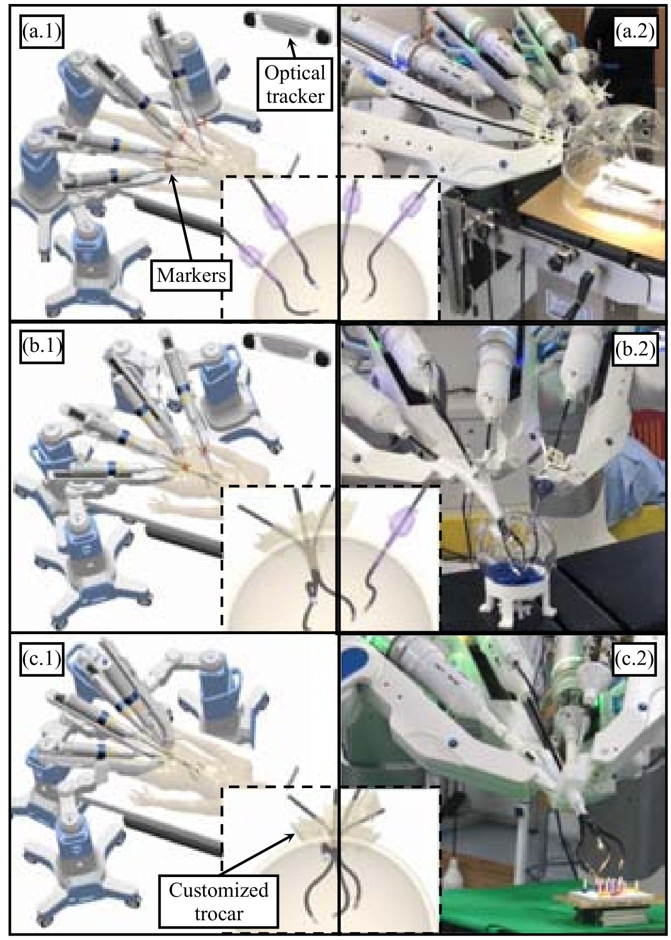

Fig. 3. Different configurations of the patient-side carts for the (a) multiport, (b) hybrid-port, and (c) single-port procedures.

the relative trocar poses. With the trocar geometry known, an optical tracker is deployed to obtain the trocars' relative poses to enable the image-guided teleoperation.

In the single-port configuration, a different four-channel trocar is designed and used. And the surgical tools are steered through the curved access channels into a patient's abdomen. In this "Y" configuration, the image-guided teleoperation only depends on the prior knowledge of the trocar geometry.

Via utilizing different accessories (e.g., the standard and the customized trocars) and different patient-side cart arrangement, the SHURUI system is, hence, expected to handle the multiport, hybrid-port, and single-port procedures.

III. System Description

The SHURUI platform consists of a surgeon console, several modular patient-side carts, an equipment cart, exchangeable surgical/endoscopic tools, and a few accessories.

A. *Endoscopic Tool, Surgical Tool, and Accessories*

As illustrated in Fig. 4, the surgical/endoscopic tool is installed on the patient-side cart. A five-DoF lockable stand poses an actuation assembly that drives the surgical/endoscopic tool.

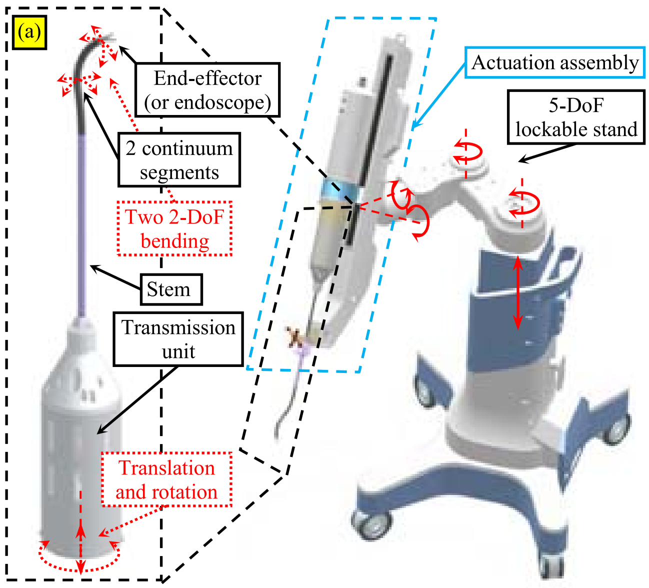

Fig. 4. Overview of the patient-side cart and the surgical/endoscopic tool: the patient-side cart includes a five-DoF lockable stand and an actuation assembly. (a) Surgical/endoscopic tool achieves six-DoF intra-abdominal motions, including two two-DoF bending, as well as a translation and a rotation of a tool.

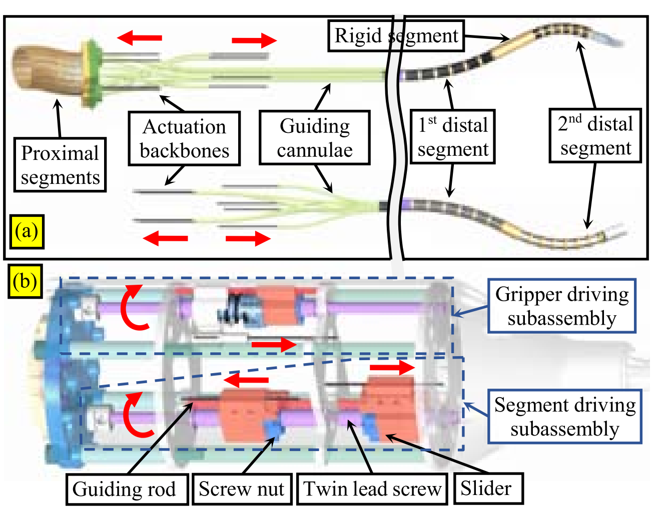

Fig. 5. Structure of the surgical/endoscopic tool: (a) structures of the continuum segments in the surgical tool (upper) and endoscopic tool (bottom) and (b) design of the transmission unit composed of four segment driving subassemblies and one gripper driving subassembly.

The surgical tool and endoscopic tool both possess two distal continuum segments, a tool stem and a transmission unit that can be detached from the actuation assembly, as outlined in Fig. 4(a). Each continuum segment can bend in arbitrary directions to provide two-DoF motions, whereas the surgical/endoscopic tool can be translated and rotated about its longitudinal axis (a.k.a., the stem axis). Six-DoF intra-abdominal motions are, hence, achieved by the tool itself.

As shown in Fig. 5(a), each distal continuum segment of the endoscopic tool is composed of four backbones made from thin nitinol rods, an end ring and several spacer rings. The backbones are attached to the end rings at the distal end, and routed into the transmission unit via the guiding cannulae at the other end. The design of dual continuum mechanisms was adopted in the surgical tools for enhanced payload capability. In total, six and 12 structural backbones are used in the first and second distal segments, respectively, and are connected to the proximal continuum segments. The proximal segments are actuated by pushing and pulling four additional actuation backbones. The adoption of the dual continuum mechanism also enables the modular actuation of the distal continuum segments with different structural parameters. The two distal continuum segments are connected by a rigid segment to enlarge the translational workspace while maintaining the tool stiffness by keeping limited segment lengths.

The central space of the continuum segments was spared for the delivery of illumination fiber, vision module signal cable, gripper actuation, etc. Silicone rubber washers were used to separate the segment spacer rings from each other. An outer tube braided from stainless steel wires was wrapped over the bending segments to enhance the segments' torsional rigidity. A fluororubber wrapping was used to cover the segment surface for smooth deployment. The outer diameter of the continuum segments in the surgical tools is 8 mm, while the outer diameter of the continuum segments in the endoscopic tool is 10 mm mainly to accommodate a pair of imaging chips and lens for the stereo vision.

The transmission unit has a uniform design for both the surgical and the endoscopic tools. As shown in Fig. 5(b), four segment driving subassemblies and one gripper driving subassembly are used to actuate both the surgical tools and the endoscopic tools. Each segment driving subassembly offers a push–pull motion for a pair of actuation backbones with a twin screw, whereas the gripper driving subassembly provides the translational motion of the gripper actuation rod by a screw.

A long stem connects the distal continuum segments and the transmission unit. The stems used in the endoscopic tool and the multiport surgical tool were rigid and straight, while the stems used in the single-port/hybrid-port surgical tool were flexible, fabricated by welding spacer rings into a stainless-steel tube with notched patterns, as shown in Fig. 6(a). When the continuum segments are fully inserted in a single-port/hybrid-port procedure, the flexible stem is passively shaped by the curved channels in the trocar while effectively transmitting axial rotation and translation for the surgical tool.

The endoscopic tool was integrated with a 3-D stereo vision module and illumination output. The 3-D vision module was composed of two side-by-side cameras (Ikegami *Tsushinki* Co. Ltd) within a ϕ10 mm diameter. Each camera has a cylindrical size of ϕ4 mm $\times$ 7 mm, and provides 60 fps video with a resolution of 1280$\times$720. The illumination was provided by an external light source via fiber optics.

Various end-effectors have been fabricated and integrated in the surgical tools, including monopolar curved scissors, monopolar cautery hooks, Maryland bipolar forceps, bipolar graspers, needle drivers, as shown in Fig. 6(b).

The trocars used in the multiport, single-port, and hybrid-port procedures are shown in Fig. 6(c.1)–(c.3). The trocars for

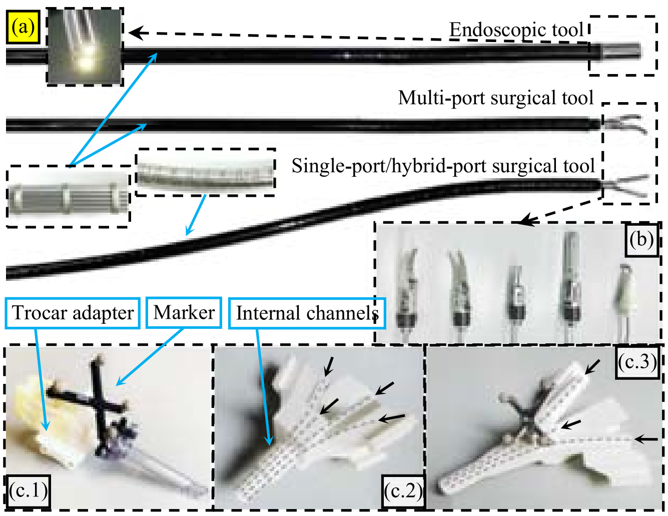

Fig. 6. Surgical/endoscopic tools and accessories for different procedures: (a) endoscopic tool and the multiport surgical tool with rigid straight stems, and the single-port/hybrid-port surgical tool with a flexible stem; (b) various surgical end-effectors (from left to right: Maryland bipolar forceps, monopolar curved scissors, needle driver, bipolar grasper, and cautery hook); and (c1)–(c3) trocars for the multiport, single-port, and hybrid-port procedures.

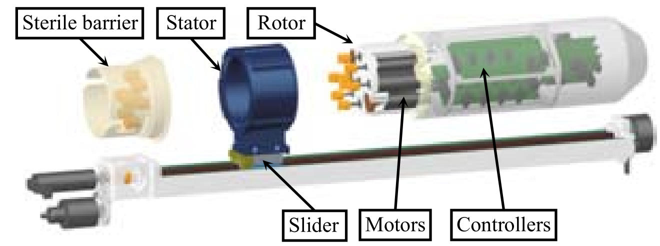

Fig. 7. Design of the actuation assembly.

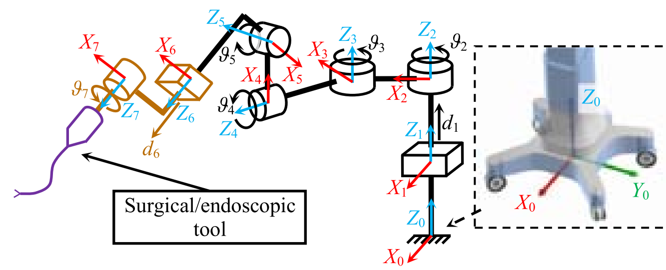

Fig. 8. Coordinate attachment of the links in the patient-side cart following the DH rule. The passive and lockable joints are represented by black, and the active joints (i.e., the ones in the actuation assembly) are represented by brown.

multiport procedures are standard bladeless trocars (B12LT, Ethicon Endo-Surgery, *LLC*), and can be connected to the patient-side cart via a 3-D printed trocar adapter. The four-channel trocar for single-port procedures and three-channel trocar for hybrid-port procedures were customized using 3-D printing. The port sizes (outer diameters) for the three-channel and four-channel trocars are 23 mm and 25 mm, respectively. These customized trocars can be used to connect three or four patient-side carts for deploying the surgical/endoscopic tools. Optical markers should be attached to the trocars for multiport and hybrid-port procedures to provide the pose relations between different trocars.

B. Patient-Side Cart

As shown in Fig. 4, each patient-side cart consists of a five-DoF lockable stand and an actuation assembly. The five-DoF lockable stand positions and orients the actuation assembly so as to deploy the installed surgical/endoscopic tools in desired configurations. The cart was designed to be a modular component of the surgical system such that only the needed number of the carts shall be pushed to the surgical bedside for preoperative setup. A minimum of three patient-carts shall be used for a MIS procedure. Moreover, the modular design enables the access of the instruments from different directions around the surgical bed, which potentially permits the anatomically optimal placement of the surgical tools and the endoscopic tool.

The lockable stand has a PRR kinematic chain with a two-DoF wrist (roll and pitch) on its distal end. All its joints are passive and lockable. Before a procedure, the incision locations and the trocar poses are determined according to the target anatomy. During the preoperative setup, a nurse can unlock the joints and maneuver the actuation assembly to spatially park the patient-side carts to the trocars at fixed instrument entry poses, by holding the handles on the actuation assembly. Further optimization of the patient-side cart placement is no required and the joints are locked to keep the patient-side carts stationary during the procedure. Details about the topological synthesis and a multilayer electromagnetic brake design of the lockable stand can be found in a previous study [29].

The actuation assembly provides six-DoF motion actuation for the surgical/endoscopic tool, and the one-DoF gripping actuation for the surgical end-effector. It is composed of a linear module and a rotary module. As shown in Fig. 7, the linear module realizes a travel of 580 mm, using a motorized lead screw. The rotary module has a rotor portion that was supported by the stator portion that is the slider of the linear module. The rotor contains six sets of servo motors and controllers. One motor actuates the rotor by having its output gear meshed with an internal gear that is attached to the stator, whereas the remaining five motors actuate the transmission unit in the surgical/endoscopic tool. The surgical/endoscopic tool is connected to the actuation assembly via the sterile barrier, after the patient-side cart has been covered with the sterile drape.

The patient-side cart can be modeled following the DH convention, as shown in Fig. 8. Given the DH parameters in Table I, the kinematics formulation for the patient-side cart can then be readily obtained.

C. Surgeon Console

The surgeon console is equipped with a 3-D display (LMD-2451TC, Sony Inc.) and two customized haptic devices that is called CombX [30]. Each CombX is made from two Geomagic TouchX devices (3-D Systems Inc.) with a customized stylus. This is a cost-effective way to achieve six-DoF inputs (positions

TABLE I
DH PARAMETERS OF THE PATIENT-SIDE CART

Index j	a_{j-1} (mm)	α_{j-1} (deg)	d_j (mm)	ϑ_j (deg)
1	0	0	[0, 300]	0
2	0	0	828.7	[−100, 100]
3	300	0	0	[−90, 90]
4	0	−90	300	[−90, 90]
5	0	−90	0	[90, 150]
6	207.3	−90	[−446, 134]	180
5	0	0	0	[−270, 270]

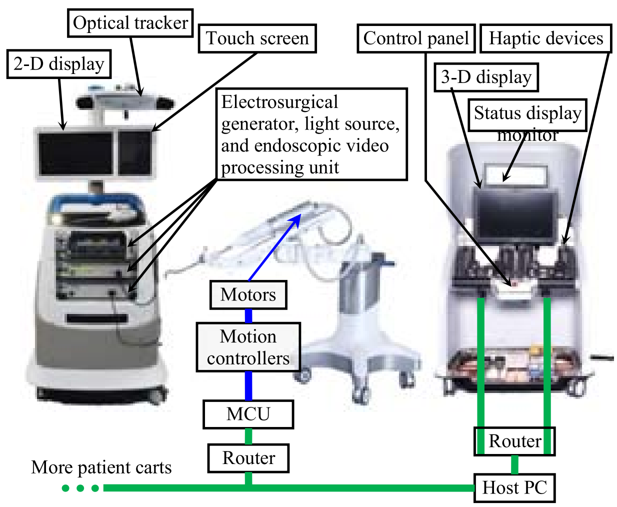

Fig. 9. Surgeon console and the equipment cart with the control infrastructure of the surgical platform.

and orientations) and five-DoF outputs (three-DoF forces and two-DoF moments). The surgeon observes the surgical site with depth perception from the 3-D display using polarized glasses. Other devices, including a control panel, switching pedals, and a system status display are also integrated, as shown in Fig. 9.

D. Equipment Cart

The equipment cart holds the equipment involved in surgical procedures, including an electrosurgical generator (e.g., the FX8 from Covidien Inc.), the endoscopic video processing unit and the light source, as shown in Fig. 9.

An optical tracker (Polaris Vega from Northern Digital Inc.) is mounted on the top of the equipment cart. It is used to obtain the poses of the trocars connected to the patient-side carts by attaching different markers to the carts. These poses are then used to register the relative poses between the surgical end-effectors and the endoscope in multiport and hybrid-port procedures, as detailed in Section IV.

The equipment cart provides another 2-D display with a touch screen to show the surgical scene and the system status to the staffs in the operating room.

E. Control Infrastructure and Software

In Fig. 9, the CombX haptic devices were connected to a host PC via a router, since the TouchX devices now use a LAN-based interface.

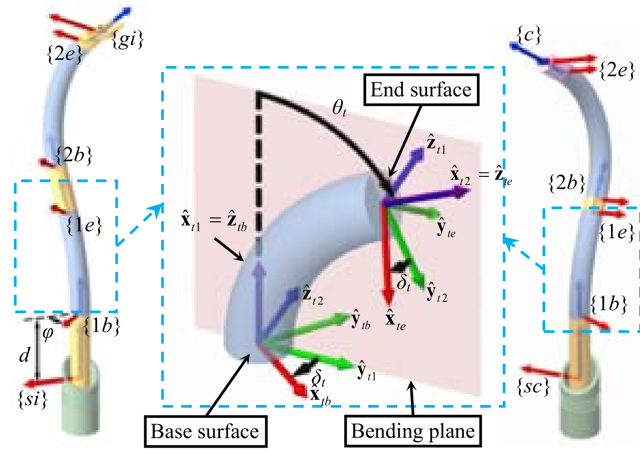

Fig. 10. Coordinates for tool kinematics, where the x-, y- and z-axes are represented with red, green, and blue arrows, respectively.

In each patient-side cart, a STM32 (STMicroelectronics Inc.) MCU (microprogrammed control unit) was connected to all the motion controllers via a CAN bus. All the MCUs are connected to the host PC via another LAN router in order to reduce the bandwidth load on the router.

The host PC with a Windows operating system runs a program with three software processes: one for the haptic devices, one for the tool kinematics, and the third for system status. The software for motion control was programmed using C++ in the Visual Studio 2019 (Microsoft Corporation) integrated development environment, and relied on the Eigen 3 template library for linear algebra computation. The kinematics process sends the inverse kinematics results to the STM32 MCUs using a user datagram protocol every 10 ms.

The STM32 MCUs runs the FreeRTOS, a real time operating system. They send the desired motor positions to the motion controllers using the CANOpen protocol.

IV. KINEMATICS AND TELEOPERATION

During teleoperation, the movement of the surgeon's hand is interpreted as target poses for the slave end-effectors of the surgical/endoscopic tools. A consistent kinematics framework is, hence, developed to handle these leader-follower scenarios in the multiport, single-port, and hybrid-port procedures.

A. Nomenclature and Coordinate Systems

The coordinate systems for the entire surgical platform are first introduced as follows to facilitate the kinematics derivation, as shown in Figs. 10 and 11.

The nomenclature is summarized in Table II.

For the tth segment, the following coordinates are defined.

1) *Base Coordinate*, $\{tb\} = \{\hat{\mathbf{x}}_{tb}, \hat{\mathbf{y}}_{tb}, \hat{\mathbf{z}}_{tb}\}$, is attached to the base surface of the tth continuum segment. The z-axis of $\{tb\}$ is normal to the base surface, and the x-axis points to a predefined direction.
2) *End Face Coordinate*, $\{te\} = \{\hat{\mathbf{x}}_{te}, \hat{\mathbf{y}}_{te}, \hat{\mathbf{z}}_{te}\}$, is attached to the center of the end surface of the tth continuum

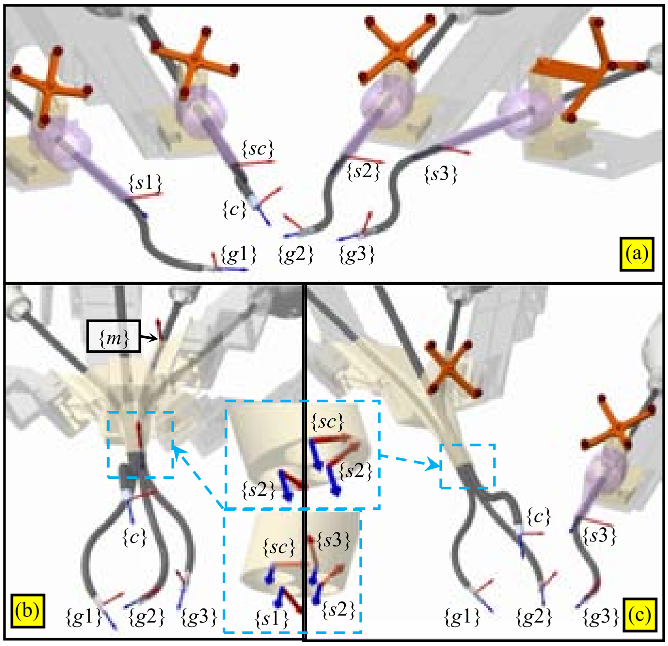

Fig. 11. Coordinates for the master-slave mapping on the slave side for: (a) multiport surgery, (b) single-port surgery, and (c) hybrid-port surgery.

TABLE II
NOMENCLATURE USED IN KINEMATICS DERIVATION

Symbol	Definition
i	Index of the surgical tools, $i = 1, 2, \ldots, N_s$.
t	Index of the continuum segments, $t = 1, 2$.
θ_t	Rotation angle of the t^{th} segment from $\hat{\mathbf{x}}_{t1}$ about $\hat{\mathbf{z}}_{t1}$ to $\hat{\mathbf{x}}_{t2}$.
δ_t	Rotation angle of the t^{th} segment from $\hat{\mathbf{y}}_{t1}$ about $\hat{\mathbf{z}}_{tb}$ to $\hat{\mathbf{x}}_{tb}$.
L_t	Lengths of the t^{th} segment.
d	Feeding length of the tool, which is the distance between the origins of $\{1b\}$ and $\{si\}$ (or $\{sc\}$).
φ	Axial rotation of the tool, which is obtained by a rotation from $\hat{\mathbf{x}}_{si}$ (or $\hat{\mathbf{x}}_{sc}$) to $\hat{\mathbf{x}}_{1b}$ about $\hat{\mathbf{z}}_{si}$ (or $\hat{\mathbf{z}}_{sc}$).
$\boldsymbol{\psi}$	$\boldsymbol{\psi} = [\varphi\ d\ \theta_1\ \delta_1\ \theta_2\ \delta_2]^T$ is the configuration vector for the surgical/endoscopic tool.
${}^b\mathbf{p}_a$, ${}^b\mathbf{R}_a$	Position vector and rotation matrix of coordinate $\{a\}$ with respect to coordinate $\{b\}$.
$\mathbf{J}_{tv}$, $\mathbf{J}_{t\omega}$	Jacobian matrices of the linear and angular velocities of the t^{th} segment.

segment. The z-axis of $\{te\}$ is normal to the end surface, and the x-axis points to the same direction as $\hat{\mathbf{x}}_{tb}$ when the segment is straight.

3) *Bending Plane Coordinate #1*, $\{t1\} = \{\hat{\mathbf{x}}_{t1}, \hat{\mathbf{y}}_{t1}, \hat{\mathbf{z}}_{t1}\}$, shares the same origin with $\{tb\}$ and aligns its x-axis with $\hat{\mathbf{z}}_{tb}$, with $\hat{\mathbf{z}}_{t1} = \hat{\mathbf{z}}_{tb} \times \hat{\mathbf{z}}_{te}$.

4) *Bending Plane Coordinate #2*, $\{t2\} = \{\hat{\mathbf{x}}_{t2}, \hat{\mathbf{y}}_{t2}, \hat{\mathbf{z}}_{t2}\}$, shares its origin with $\{te\}$ and aligns its x-axis with $\hat{\mathbf{z}}_{te}$, with $\hat{\mathbf{z}}_{t2} = \hat{\mathbf{z}}_{tb} \times \hat{\mathbf{z}}_{te}$.

For teleoperation, the following coordinates are defined.

1) *End-effector coordinate*, $\{gi\} = \{\hat{\mathbf{x}}_{gi}, \hat{\mathbf{y}}_{gi}, \hat{\mathbf{z}}_{gi}\}$, is attached to the ith surgical end-effector. $\{gi\}$ has a fixed known relation with the corresponding $\{2e\}$ of the ith instrument.

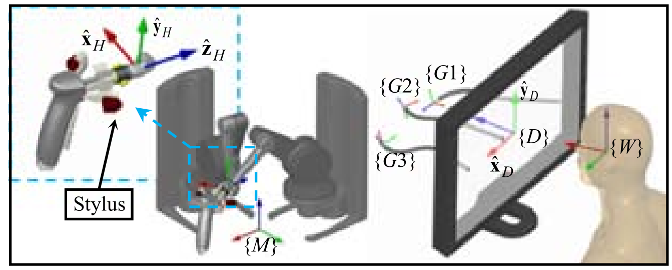

Fig. 12. Coordinates for master-slave mapping on the master side.

2) *Endoscope coordinate*, $\{c\} = \{\hat{\mathbf{x}}_c, \hat{\mathbf{y}}_c, \hat{\mathbf{z}}_c\}$, is attached to the stereo vision module of the endoscopic tool. The z-axis of $\{c\}$ is aligned with $\hat{\mathbf{z}}_{2e}$, and the x-axis of $\{c\}$ points from one optical center of the cameras to the other.

3) *Module coordinate*, $\{m\} = \{\hat{\mathbf{x}}_m, \hat{\mathbf{y}}_m, \hat{\mathbf{z}}_m\}$, is attached to the linear module with its origin located at the entry point of the trocar. As shown in Fig. 11(b), the z-axis points to the insertion direction of the surgical tool, whereas the x-axis indicates the zero axial rotation of the tool.

4) *Trocar sleeve coordinate*, $\{si\} = \{\hat{\mathbf{x}}_{si}, \hat{\mathbf{y}}_{si}, \hat{\mathbf{z}}_{si}\}$ or $\{sc\} = \{\hat{\mathbf{x}}_{sc}, \hat{\mathbf{y}}_{sc}, \hat{\mathbf{z}}_{sc}\}$, is attached to the trocar sleeve corresponding to the ith surgical tool or the endoscopic tool. They are the reference coordinates for the tools' intracorporeal motions. $\{si\}$ or $\{sc\}$ is defined by moving $\{m\}$ along the lumen's centerline while keeping the z-axis tangent to the centerline without twisting.

On the master side, another set of coordinates, which are designated using capital letters, are used to denote the spatial relations between the devices on the surgeon console, as shown in Fig. 12.

1) *User coordinate*, $\{W\} = \{\hat{\mathbf{x}}_W, \hat{\mathbf{y}}_W, \hat{\mathbf{z}}_W\}$, is aligned with a user and used as the motion reference on the master side.

2) *Master base coordinate*, $\{M\} = \{\hat{\mathbf{x}}_M, \hat{\mathbf{y}}_M, \hat{\mathbf{z}}_M\}$, refers to the coordinate attached to the base of the left or the right haptic device.

3) *Master stylus coordinate*, $\{H\} = \{\hat{\mathbf{x}}_H, \hat{\mathbf{y}}_H, \hat{\mathbf{z}}_H\}$, is attached to the stylus of the left or the right haptic device. The z-axis of $\{H\}$ coincides with the stylus central axis.

4) *Display coordinate*, $\{D\} = \{\hat{\mathbf{x}}_D, \hat{\mathbf{y}}_D, \hat{\mathbf{z}}_D\}$, is attached to the 3-D display. The xy plane coincides with the screen, with $\hat{\mathbf{y}}_D$ pointing upwards and $\hat{\mathbf{z}}_D$ pointing inwards the screen.

5) *Imaginary end-effector coordinate*, $\{Gi\} = \{\hat{\mathbf{x}}_{Gi}, \hat{\mathbf{y}}_{Gi}, \hat{\mathbf{z}}_{Gi}\}$, is the imaginary coordinate corresponding to ith end-effector coordinates $\{gi\}$.

B. Tool Kinematics

The kinematics model for the surgical tool is developed based on the assumption that each continuum segment bends with constant curvature. The kinematic variables are the bending angles θ_t ($t = 1, 2$), bending direction angles δ_t ($t = 1, 2$), tool translation length d, and tool axial rotation angle φ, as shown

This article has been accepted for inclusion in a future issue of this journal. Content is final as presented, with the exception of pagination.

TABLE III
KEY STRUCTURAL PARAMETERS OF CONTINUUM ARMS

	L_1 (mm)	L_2 (mm)	L_r (mm)	θ_1 (rad)	θ_2 (rad)
Endoscopic tool	40	60	10	[0, π/2]	[0, 2π/3]
Multi-port surgical tool	40	60	10	[0, π/2]	[0, 3π/4]
Single-port/ hybrid-port surgical tool	70	60	10	[0, π/2]	[0, 3π/4]

in Fig. 10. The detailed kinematics model for the proposed continuum arm can be referred to [31]. A brief description is presented here for completeness.

For the tth continuum segment, the position and orientation of $\{te\}$ with respect to $\{tb\}$ are given by

$$^{tb}\mathbf{p}_{te} = \frac{L_t}{\theta_t}[\cos\delta_t(1-\cos\theta_t)\sin\delta_t(\cos\theta_t-1)\sin\theta_t]^T \quad (1)$$

$$^{tb}\mathbf{R}_{te} = \mathrm{Rot}(\hat{\mathbf{z}}_{tb}, -\delta_t)\mathrm{Rot}(\hat{\mathbf{z}}_{t1}, \theta_t)\mathrm{Rot}(\hat{\mathbf{z}}_{te}, \delta_t) \quad (2)$$

where $^{tb}\mathbf{p}_{te}$= [00 L_t]^T when $\theta_t \to 0$; $\mathrm{Rot}(\hat{\mathbf{n}}, \alpha)$represents the rotation matrix about $\hat{\mathbf{n}}$ axis by an angle α.

The direct kinematics that maps the configuration vector ψ to the pose of $\{gi\}$ is obtained as follows:

$$^{si}\mathbf{p}_{gi} = {}^{si}\mathbf{R}_{1b}\left({}^{1b}\mathbf{R}_{1e}\left({}^{1e}\mathbf{R}_{2e}{}^{2e}\mathbf{p}_{gi} + {}^{1e}\mathbf{p}_{2e}\right) + {}^{1b}\mathbf{p}_{1e}\right) + {}^{si}\mathbf{p}_{1b} \quad (3)$$

$$^{si}\mathbf{R}_{gi} = {}^{si}\mathbf{R}_{1b}{}^{1b}\mathbf{R}_{1e}{}^{1e}\mathbf{R}_{2b}{}^{2b}\mathbf{R}_{2e}{}^{2e}\mathbf{R}_{gi} \quad (4)$$

where $^{si}\mathbf{R}_{1b} = \mathrm{Rot}(\hat{\mathbf{z}}_s, \varphi)$ and $^{si}\mathbf{p}_{1b} = [0\ 0\ d]^T$ represent the rotation and translation of the tool; $^{2e}\mathbf{R}_{gi} = {}^{1e}\mathbf{R}_{2b} = \mathbf{I}_{3\times3}$, $^{2e}\mathbf{p}_{gi}$ = [00 L_g]^T, and $^{1e}\mathbf{p}_{2b}$ = [00 L_r]^T are known structure parameters of the end-effector and the rigid segment, respectively.

The linear velocity and angular velocity Jacobian matrices for the tth continuum segment are $\mathbf{J}_{tv}$ and $\mathbf{J}_{t\omega}$, respectively, and the Jacobian matrices for the rotation and translation of the tool are denoted by $\mathbf{J}_\varphi$ and $\mathbf{J}_d$, respectively. The formulation of these matrices can be referred to [31].

For the surgical tool, the twist of coordinate $\{gi\}$ with respect to $\{si\}$ is given as follows:

$$\dot{\mathbf{x}} = \mathbf{J}\dot{\psi} = \begin{bmatrix} \mathbf{W}_1 & {}^{si}\mathbf{R}_{1b}\mathbf{W}_2 & {}^{si}\mathbf{R}_{2b}\mathbf{W}_3 \\ \mathbf{J}_\varphi & {}^{si}\mathbf{R}_{1b}\mathbf{J}_{1\omega} & {}^{si}\mathbf{R}_{2b}\mathbf{J}_{2\omega} \end{bmatrix}\dot{\psi} \quad (5)$$

where $\mathbf{W}_1 = \mathbf{J}_d - [{}^{si}\mathbf{R}_{1b}{}^{1b}\mathbf{p}_{gi}]^\wedge\mathbf{J}_\varphi$, $\mathbf{W}_2 = \mathbf{J}_{1v} - [{}^{1b}\mathbf{R}_{1e}{}^{1e}\mathbf{p}_{gi}]^\wedge\mathbf{J}_{1\omega}$, and $\mathbf{W}_3 = \mathbf{J}_{2v} - [{}^{2b}\mathbf{R}_{2e}{}^{1e}\mathbf{p}_{gi}]^\wedge\mathbf{J}_{2\omega}$; The operator $[\bullet]^\wedge$ converts an element in $\mathbb{R}^3$ to its corresponding element in so(3).

The actuation kinematics that relates the backbone actuation lengths and the configuration variables can be referred to [25].

The kinematics model for the endoscopic tool has the same formulation as in (1) to (11), with the subscript $(\bullet)_{gi}$ replaced by $(\bullet)_c$, and the superscript $^{si}(\bullet)$ replaced by $^{sc}(\bullet)$.

Based on the aforementioned tool kinematics, the lengths of the segments was refined using the optimization framework that aims at improving the manipulator's distal dexterity [31], [32], provided the constraints on total segment lengths, maximum bending curvatures, and target workspaces. The key structural parameters that are rounded for manufacturing purposes for different tools are listed in Table III.

C. Teleoperation of the Surgical Tools

To conduct the teleoperation, the first step is to establish the matching between the haptic device and one of the surgical tools. At this stage, the CombX actively aligns its stylus's orientation in accordance to the orientation of the target end-effector.

During the teleoperation of surgical tools, the endoscopic tool is assumed stationary. An intuitive teleoperation requires the motion of the imaginary surgical end-effector perceived by the user follows the motion of the user's hand. Hence, the linear motions of the stylus $\{H\}$ and the imaginary surgical end-effector $\{Gi\}$ on the 3-D display can be set proportional, while their rotational motions shall be the same, which can be expressed as follows:

$$^W\mathbf{p}_{Gi} - {}^W\mathbf{p}_{Gi*} = k\left({}^W\mathbf{p}_H - {}^W\mathbf{p}_{H*}\right) \quad (6)$$

$$^W\mathbf{R}_{Gi}{}^W\mathbf{R}_{Gi*}^T = {}^W\mathbf{R}_H{}^W\mathbf{R}_{H*}^T \quad (7)$$

where k is an adjustable teleoperation scaling factor; the asterisk $(\bullet)^*$ is used to denote the coordinate at the initial time of the teleoperation when the haptic device and surgical tool match. Hence, (6) and (7) relate the relative motions of the stylus and the imaginary surgical end-effector with respect to their initial states.

Ideally, the pose relation between the imaginary end-effector $\{Gi\}$ and the 3-D display $\{D\}$ represents the exact orientation relation and the scaled position relation between $\{gi\}$ and $\{c\}$. This will be employed to formulate the kinematic connection between the master side and the slave side

$$^D\mathbf{R}_{Gi} = {}^c\mathbf{R}_{gi} = {}^c\mathbf{R}_{sc}{}^{sc}\mathbf{R}_{si}{}^{si}\mathbf{R}_{gi} \quad (8)$$

$$\eta^D\mathbf{p}_{Gi} = {}^c\mathbf{p}_{gi} = {}^c\mathbf{p}_{sc} + {}^c\mathbf{R}_{sc}{}^{sc}\mathbf{p}_{si} + {}^c\mathbf{R}_{sc}{}^{sc}\mathbf{R}_{si}{}^{si}\mathbf{p}_{gi} \quad (9)$$

where η is a scaling factor that is affected by the perceived movements of the imaginary tool end-effector on the display (e.g., different sizes of the display may affect this factor).

Substituting $^W\mathbf{R}_{Gi}$ and $^W\mathbf{p}_{Gi}$ in (6) and (7) using (8) and (9) yields

$$^{si}\mathbf{p}_{gi} = k\eta\cdot({}^{si}\mathbf{R}_{sc}{}^{sc}\mathbf{R}_c{}^D\mathbf{R}_M)\left({}^M\mathbf{p}_H - {}^M\mathbf{p}_{H*}\right) + {}^{si}\mathbf{p}_{gi*} \quad (10)$$

$$^{si}\mathbf{R}_{gi} = ({}^{si}\mathbf{R}_{sc}{}^{sc}\mathbf{R}_c{}^D\mathbf{R}_M)^M\mathbf{R}_H{}^{H*}\mathbf{R}_{Gi*} \quad (11)$$

where the initial positions $^{si}\mathbf{p}_{gi*}$ and $^M\mathbf{p}_{H*}$ and orientation $^{H*}\mathbf{R}_{Gi*}$ are recorded at the matching instant, and $^D\mathbf{R}_M$ is from the known arrangement of the haptic device and the 3-D display.

Equations (10) and (11) describe the relations between the haptic device input $^M\mathbf{p}_H$, $^M\mathbf{R}_H$, and the end-effector output $^{si}\mathbf{p}_{gi}$, $^{si}\mathbf{R}_{gi}$. The relation relies on the relative orientations $^D\mathbf{R}_M$, as well as $^{sc}\mathbf{R}_c$ (obtained from kinematics of the endoscopic tool) and $^{si}\mathbf{R}_{sc}$, which is obtained as follows:

The way to obtain the relation between the trocar sleeve coordinates $\{si\}$ and $\{sc\}$ depends on the adopted patient-side configuration in the surgical procedure. For multiport procedures, the poses of $\{si\}$ and $\{sc\}$ are first related to the poses of the optical markers attached to the standard trocars, and the pose relations among these markers are offered by the optical tracker on the equipment cart. For hybrid-port procedures, the pose relation between $\{si\}$ and $\{sc\}$ that are both attached to the customized three-channel trocar is obtained from the prior knowledge of the geometry of the trocar, while the pose relation between $\{si\}$ and $\{sc\}$ attached to different trocars can be related using the optical tracker. For single-port procedures, the geometry of the customized four-channel trocar is enough to obtain the pose relations between $\{si\}$ and $\{sc\}$.

D. Teleoperation of the Endoscopic Tool

The user can change his/her control target from the surgical tools to the endoscopic tool by a switching pedal. Then, the surgeon can steer the endoscope for a desired viewing angle. Different from the master-slave mapping for the surgical tools, the motion of the stylus indicates the opposite motion of the scene in the endoscopic image. This means the incremental motion of the stylus shall be mapped to the incremental motion of the stereo module with respect to itself, as formulated by

$$ {}^{c^-}\mathbf{p}_c = k\left({}^{W}\mathbf{p}_H - {}^{W}\mathbf{p}_{H^-}\right) \tag{12}$$

$$ {}^{c^-}\mathbf{R}_c = {}^{W}\mathbf{R}_H {}^{W}\mathbf{R}_{H^-}^T \tag{13}$$

where $(\bullet)^-$ represents the current state of the coordinate.

The pose relation between the stylus $\{H^-\}$ and the master base $\{M\}$, and between the endoscope $\{c^-\}$ and the corresponding trocar sleeve $\{sc\}$, are recorded in every control cycle during the teleoperation of the endoscopic tool. The movement target for the stereo module is, hence, specified by

$$ {}^{sc}\mathbf{p}_c = k \cdot {}^{sc}\mathbf{R}_{c^-} {}^{W}\mathbf{R}_M \left({}^{M}\mathbf{p}_H - {}^{M}\mathbf{p}_{H^-}\right) + {}^{sc}\mathbf{p}_{c^-} \tag{14}$$

$$ {}^{sc}\mathbf{R}_c = {}^{sc}\mathbf{R}_{c^-}\left({}^{W}\mathbf{R}_M {}^{M}\mathbf{R}_H\right)\left({}^{W}\mathbf{R}_M {}^{M}\mathbf{R}_{H^-}\right)^T. \tag{15}$$

In summary, the target poses of the surgical tool or the endoscopic tool with respect to the trocar sleeve coordinate are specified by the stylus using (10), (11) or (14), (15), respectively. The assumed actual poses of $\{gi\}$ or $\{c\}$ are calculated from the tool's forward kinematics in (1)–(4), since there are no shape sensors in the surgical or endoscopic tools. The differences between the actual and the target poses are used to determine the task space twist $\dot{\mathbf{x}}$, and hence, the configuration velocity can be obtained by the inverse kinematics in

$$ \dot{\psi} = \begin{cases} \mathbf{J}^T\left(\mathbf{J}\mathbf{J}^T + \lambda\mathbf{I}\right)\dot{\mathbf{x}}, & \sigma_{\min} < \varepsilon \\ \mathbf{J}^T\left(\mathbf{J}\mathbf{J}^T\right)^{-1}\dot{\mathbf{x}}, & \text{otherwise} \end{cases} \tag{16}$$

where $\sigma_{\min}$ is the nonzero smallest singular value of $\mathbf{J}$, and λ and ε are small positive values.

V. Experimental Validations

Several experiments were conducted to demonstrate the performance and potentials of the SHURUI platform, as well as to validate its compatibility for different surgical paradigms.

A. Motion Calibration

To compensate the shape discrepancy between the actual and the ideal bending of the continuum segments, experiments were conducted to calibrate the bending of the continuum segments, referring to prior studies [25], [33]. The compensated bending angle $\tilde{\theta}_t$ is, hence, formulated in

$$ \tilde{\theta}_t = \begin{cases} e_{t,\text{bd}}\theta_t, & \dot{\theta}_t > 0 \\ e_{t,\text{st}}\theta_t, & \dot{\theta}_t < 0 \end{cases} \tag{17}$$

where $e_{t,\text{bd}}$ and $e_{t,\text{st}}$ represents the coefficients for bending and straightening of the tth segment. The values of $e_{t,\text{bd}}$ and $e_{t,\text{st}}$ are available in Table IV.

TABLE IV
Values of Compensation Coefficients

Multi-port surgical tool		Single-port/hybrid-port surgical tool	
$e_{1,\text{bt}} = 1.399$	$e_{1,\text{st}} = 1.273$	$e_{1,\text{bt}} = 1.493$	$e_{1,\text{st}} = 1.292$
$e_{2,\text{bt}} = 1.240$	$e_{2,\text{st}} = 1.110$	$e_{2,\text{bt}} = 1.302$	$e_{2,\text{st}} = 1.097$

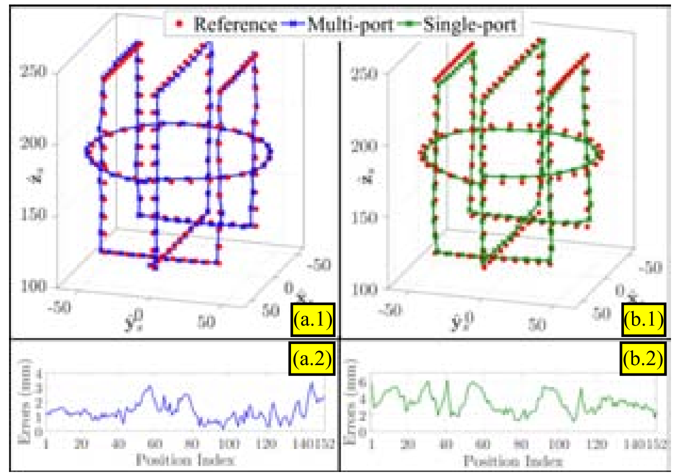

Fig. 13. Positioning accuracy tests for (a) the multiport surgical tool and (b) the single-port/hybrid-port surgical tool. The actual and reference positions are in the upper plots, and the corresponding errors were in bottom plots.

Tip positioning accuracies of multiport and single-port/hybrid-port surgical tools were then tested to validate the results for the actuation compensation. A set of points in a ϕ120 mm $\times$ 120 mm cylindrical volume was chosen as the target positions to reach. The actual tip positions were obtained using another optical tracker (Micron Tracker SX60, Claron Technology Inc.) and were compared to the reference target positions. The results for the multiport surgical tool and the single-port surgical tool are presented in Fig. 13(a.1) and (b.1), and the corresponding positioning errors for each point are shown in Fig. 13(a.2) and (b.2). The average positioning errors were 1.34 mm and 3.47 mm for the multiport surgical tool and the single-port surgical tool, respectively, and the corresponding maximum errors were 3.33 mm and 6.17 mm.

B. Payload Capability Tests

To quantify the payload capability of the surgical tools with the dual continuum mechanism design, tip-loading experiments were conducted on the surgical tools. The surgical tool was first commanded to one of the following three poses, as in Fig. 14:

$$ \psi_1 : [\,\varphi = 0\; d = 0\; \theta_1 = 0\; \delta_1 = 0\; \theta_2 = 0\; \delta_2 = 0]^T $$

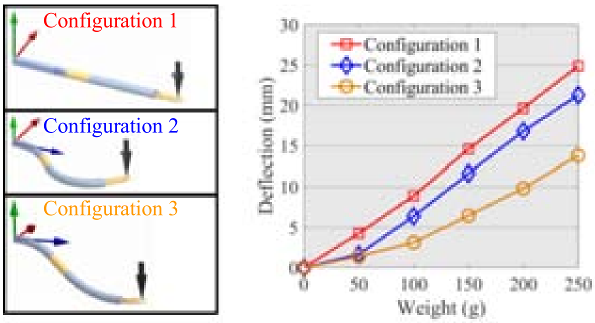

Fig. 14. Deflections of the end-effector loaded by weights in different poses.

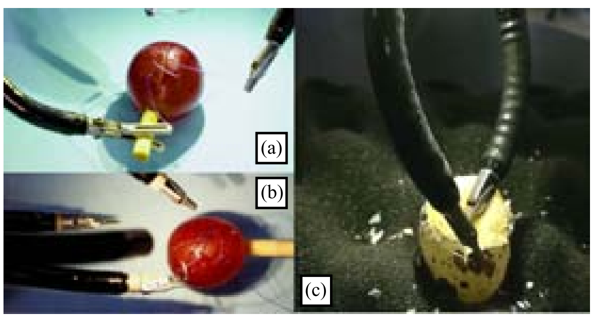

Fig. 15. Suturing and peeling tasks: (a) multiport suturing, (b) single-port suturing, and (c) peeling a quail eggshell without damaging the membrane.

$$\psi_2 : [\ \varphi = 0\ d = 0\ \theta_1 = \pi/4\ \delta_1 = \pi\ \theta_2 = \pi/2\ \delta_2 = 0]^T$$
$$\psi_3 : [\ \varphi{=}0\ d{=}0\ \theta_1{=}\pi/4\ \delta_1{=}\pi/2\ \theta_2{=}\pi/4\ \delta_2{=}{-}\pi/2]^T.$$

Several weights were then added to the end-effector of the surgical tool. The deflections of the continuum segments were obtained also using the optical tracker and customized markers.

The tip deflection values against the weight are plotted in Fig. 14. The deflections were considered small (less than 10% of the total protruded total length of the segments) when the weight was lighter than 150 g. The results exhibited improvement compared to the payload capability of the previous SURS system in [25], due to the larger tool diameter (8.0 mm versus 6.5 mm) and more arranged backbones. This deflection can be actively corrected by the surgeon under 3-D visual feedback during teleoperation. Although the continuum segments underwent intensive deflection when the weight continued to increase, they were still capable of exerting sufficient forces when the accuracy was not a prior consideration (e.g., tightening a thread).

C. Surgical Task Simulations

A number of demonstrative experiments were conducted on the SHURUI system to validate its ability to accomplish surgical tasks for multiport and single-port procedures. Tasks of suturing grapes and shell-peeling of quail eggs were performed, as shown in Fig. 15. Video clips for these processes are included in the multimedia extension. The system was able to suture in both multiport and single-port paradigms, and to peel the quail eggshell without damaging the membrane. These experiments exhibited the satisfactory accuracy and dexterity of the system for both multiport and single-port procedures.

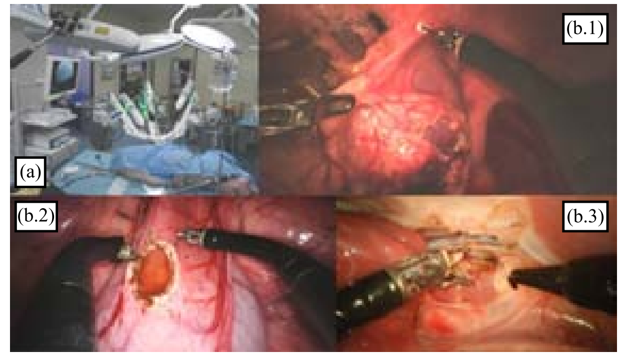

Fig. 16. Animal studies: (a) arrangements of the SHURUI platform in the operating room, and the endoscopic views of (b.1) single-port laparoscopic radical nephrectomy, (b.2) single-port partial bladder resection and suturing, and (b.3) single-port thoracoscopic lymph node dissection. Please also refer to the attached multimedia extension.

D. Animal Studies

A series of nonsurvival experiments were carried out on porcine models to assess the system's performance in realistic clinical settings for different surgical paradigms. The porcine models weighing from 45 kg to 55 kg were used. The animal studies were approved by the Shanghai Yinshe clinical center, which is a qualified company to issue ethics certification and offer sites for animal studies.

The experiments included a single-port laparoscopic radical nephrectomy (LRN), a single-port laparoscopic partial bladder resection and suturing, and a single-port thoracoscopic mediastinal lymph node dissection, as shown in Fig. 16. Before the procedures, the porcine models were anesthetized.

In the LRN procedure, the porcine model was put in a lateral decubitus pose and the incision was made near the position close to a human's umbilicus. A dissector, and a bipolar grasper and a monopolar scissors were used to free the whole kidney from the surrounding tissues. The renal artery and ureter were resected after the Hem-o-lok clips were applied. The LRN procedure demonstrated the surgical tools' ability to apply sufficient forces and cover adequate surgical sites, even reaching the obstructed locations behind the kidney.

In the partial bladder resection procedure, the porcine model was put in a supine pose. Target tissues on the bladder wall were first lifted by forceps and resected by a monopolar scissors. After the removal of the target tissues, the monopolar scissors were switched to a needle driver to close the cut on the bladder. A clip was applied to replace a knot. This technique was widely adopted clinically.

An ancillary port was also made in the urologic procedures to deploy assistive instruments (e.g., clip applier and suction tool).

In the mediastinal lymph node dissection procedure, the porcine model was put in a supine pose and the access to the thoracic cavity is made under the xiphisternum. A lymph node was identified and dissected using a dissector and a cautery hook, after a nearby artery was separated from the tissues. The surgical tasks were completed under severe disturbances on the continuum segments from the beating heart.

In all the aforementioned procedures, the trocars were placed first. Then, the patient-side carts were pushed in place and connected to the trocars.

The operation durations for the urologic procedures were both about 80 min, whereas the thoracic procedure costed about 70 min. The operation duration was counted from opening the incision to closing the incision. The setup time for the nephrectomy, bladder resection and suturing, and mediastinal lymph node dissection was about 30 to 40 min. Since the operation time and the setup time are subject to future usability studies, the durations were not precisely timed. During these procedures, the intraoperative vital signs such as the heart rate, respiratory rate, blood oxygen saturation, blood pressure, and body temperature were within normal ranges, showing the SHURUI system's ability to meet the clinical needs in a realistic clinical setting. Video clips showing the endoscopic views of these procedures are included in the multimedia extension.

VI. Conclusion

This article presents the design, system description, kinematics, teleoperation framework, and experimental characterizations of the SHURUI surgical system, a modular robotic platform for handling multiport, single-port, and for the first time, hybrid-port procedures. Modular patient-side carts are used to deploy the surgical/endoscopic tools via accessing ports that can be arranged with a high level of freedom. This feature can potentially provide surgical treatments to patients with a suitable level of invasiveness, where only the required number incisions are to be made.

A series of experimental characterizations were carried out to demonstrate the features of the SHURUI platform. The achieved positioning accuracy of 1.34 mm for the multiport surgical tools, and 3.47 mm for the single-port surgical tools after actuation compensation was consider satisfactory. And the payload tests showed that the surgical tool was deflected in acceptable ranges when the load was mild. The success in carrying out the mockup surgical tasks and the animal studies verified that the accuracy, the dexterity, and the payload capability of the SHURUI system have met the clinical needs.

True potentials of the SHURUI platform are to be confirmed on larger scale animal studies and even clinical trials. Several aspects for future improvements were also identified. For example, the patient-side cart can be more compact to reduce the footprint during usage. What's more, mechanics-based modeling approaches and shape sensing techniques can be explored to further improve the tool's posing accuracy and even realize closed-loop control.

References

[1] R. H. Taylor, "A perspective on medical robotics," *Proc. IEEE*, vol. 94, no. 9, pp. 1652–1664, Sep. 2006.

[2] C. Bergeles and G.-Z. Yang, "From passive tool holders to microsurgeons: Safer, smaller, smarter surgical robots," *IEEE Trans. Biomed. Eng.*, vol. 61, no. 5, pp. 1565–1576, May 2014.

[3] Y. Chen, S. Zhang, Z. Wu, B. Yang, Q. Luo, and K. Xu, "A review of surgical robotic systems for keyhole and endoscopic procedures: State of the art and perspectives," *Front. Med.*, vol. 14, pp. 382–403, 2020.

[4] G. S. Guthart and J. K. Salisbury, "The intuitive^{TM} telesurgery system: Overview and application," in *Proc. IEEE Int. Conf. Robot. Autom.*, 2000, pp. 618–621.

[5] H. Takahashi, S. Warisawa, M. Mitsuishi, J. Arata, and M. Hashizume, "Development of high dexterity minimally invasive surgical system with augmented force feedback capability," in *Proc. IEEE/RAS-EMBS Int. Conf. Biomed. Robot. Biomechatronics*, 2006, pp. 284–289.

[6] M. B. Hong and Y.-H. Jo, "Design of a novel 4-DOF wrist-type surgical instrument with enhanced rigidity and dexterity," *IEEE/ASME Trans. Mechatronics*, vol. 19, no. 2, pp. 500–511, Apr. 2014.

[7] P. Berkelman and J. Ma, "A compact modular teleoperated robotic system for laparoscopic surgery," *Int. J. Robot. Res.*, vol. 28, no. 9, pp. 1198–1215, 2009.

[8] Z. Dai, Z. Wu, J. Zhao, and K. Xu, "A robotic laparoscopic tool with enhanced capabilities and modular actuation," *Sci. China Technol. Sci.*, vol. 62, no. 1, pp. 47–59, 2019.

[9] J. Arata *et al.*, "Compliant four degree-of-freedom manipulator with locally deformable elastic elements for minimally invasive surgery," in *Proc. IEEE Int. Conf. Robot. Autom.*, 2019, pp. 2663–2669.

[10] C. Freschi, V. Ferrari, F. Melfi, M. Ferrari, F. Mosca, and A. Cuschieri, "Technical review of the da Vinci surgical telemanipulator," *Int. J. Med. Robot. Comput. Assist. Surgery*, vol. 9, no. 4, pp. 396–406, Dec. 2013.

[11] U. Kim, D.-H. Lee, Y. B. Kim, D.-Y. Seok, J. So, and H. R. Choi, "S-Surge: Novel portable surgical robot with multiaxis force-sensing capability for minimally invasive surgery," *IEEE/ASME Trans. Mechatronics*, vol. 22, no. 4, pp. 1717–1727, Aug. 2017.

[12] B. Hannaford *et al.*, "Raven-II: An open platform for surgical robotics research," *IEEE Trans. Biomed. Eng.*, vol. 60, no. 4, pp. 954–959, Apr. 2013.

[13] S. E. Bunter and M. Ghodoussi, "Transforming a surgical robot for human telesurgery," *IEEE Trans. Robot. Automat.*, vol. 19, no. 5, pp. 818–824, Oct. 2003.

[14] M. M. Dalvand and B. Shirinzadeh, "Remote centre-of-motion control algorithms of 6-RRCRR parallel robot assisted surgery system (PRAMiSS)," in *Proc. IEEE Int. Conf. Robot. Autom.*, 2012, pp. 3401–3406.

[15] M. A. Nasseri *et al.*, "Virtual fixture control of a hybrid parallel-serial robot for assisting ophthalmic surgery: An experimental study," in *Proc. IEEE /RAS-EMBS Int. Conf. Biomed. Robot. Biomechatronics*, 2014, pp. 732–738.

[16] G. Navarra, E. Pozza, S. Occhionorelli, P. Carcoforo, and I. Donini, "One-wound laparoscopic cholecystectomy," *Brit. J. Surgery*, vol. 84, no. 5, pp. 695–695, 1997.

[17] M. Hwang *et al.*, "A single port surgical robot system with novel elbow joint mechanism for high force transmission," *Int. J. Med. Robot. Comput. Assist. Surgery*, vol. 13, no. 4, Dec. 2017, Art. no. e1808.

[18] O. J. Isaac-Lowry, S. Okamoto, S. A. Pedram, R. Woo, and P. Berkelman, "Compact teleoperated laparoendoscopic single-site robotic surgical system: Kinematics, control, and operation," *Int. J. Med. Robot. Comput. Assist. Surgery*, vol. 13, no. 4, Dec. 2017, Art. no. e1811.

[19] J. H. Kaouk *et al.*, "A novel robotic system for single-port urologic surgery: First clinical investigation," *Eur. Urology*, vol. 66, no. 6, pp. 1033–1043, Dec. 2014.

[20] B. Seeliger, M. Diana, J. P. Ruurda, K. M. Konstantinidis, J. Marescaux, and L. L. Swanström, "Enabling single-site laparoscopy: The SPORT platform," *Surgical Endoscopy*, vol. 33, pp. 3696–3703, Jan. 2019.

[21] T. D. Wortman, J. M. Mondry, S. M. Farritor, and D. Oleynikov, "Single-site colectomy with miniature in vivo robotic platform," *IEEE Trans. Biomed. Eng.*, vol. 60, no. 4, pp. 926–929, Apr. 2013.

[22] C. Quaglia, G. Petroni, M. Niccolini, S. Caccavaro, P. Dario, and A. Menciassi, "Design of a compact robotic manipulator for single-port laparoscopy," *J. Mech. Des.*, vol. 136, no. 10, Oct. 2014, Art. no. 105001.

[23] Y. Kobayashi *et al.*, "Development of a robotic system with six-degrees-of-freedom robotic tool manipulators for single-port surgery," *Int. J. Med. Robot. Comput. Assist. Surgery*, vol. 11, no. 2, pp. 235–246, Jun. 2015.

[24] J. Ding, R. E. Goldman, K. Xu, P. K. Allen, D. L. Fowler, and N. Simaan, "Design and coordination kinematics of an insertable robotic effectors platform for single-port access surgery," *IEEE/ASME Trans. Mechatronics*, vol. 18, no. 5, pp. 1612–1624, Oct. 2013.

[25] K. Xu, J. Zhao, and M. Fu, "Development of the SJTU unfoldable robotic system (SURS) for single port laparoscopy," *IEEE/ASME Trans. Mechatronics*, vol. 20, no. 5, pp. 2133–2145, Oct. 2015.

[26] B. J. Champagne *et al.*, "Single-incision versus standard multiport laparoscopic colectomy: A multicenter, case-controlled comparison," *Ann. Surgery*, vol. 255, no. 1, pp. 66–69, Jan. 2012.

[27] N. Tamini *et al.*, "Single-incision versus standard multiple-incision laparoscopic cholecystectomy: A meta-analysis of experimental and observational studies," *Surgery Innov.*, vol. 21, no. 5, pp. 528–545, Oct. 2014.

[28] G.-P. Haber *et al.*, "Novel robotic da Vinci instruments for laparoendoscopic single-site surgery," *Urology*, vol. 76, no. 6, pp. 1279–1282, Dec. 2010.

[29] T. Dong, Y. Chen, L. Zeng, Z. Liu, and K. Xu, "Design and validation of multi-layer brakes for a lockable stand for a surgical robotic system," in *Proc. IEEE Int. Conf. Robot. Biomimetics*, 2018, pp. 1244–1249.

[30] B. Zhao, S. Zhang, Z. Wu, B. Yang, and K. Xu, "CombX: Design and experimental characterizations of a haptic device for surgical teleoperation," *Int. J. Med. Robot. Comput. Assist. Surgery*, vol. 16, no. 1, Feb. 2020, Art. no. e2042.

[31] S. Zhang, Q. Li, H. Yang, J. Zhao, and K. Xu, "Configuration transition control of a continuum surgical manipulator for improved kinematic performance," *IEEE Robot. Autom. Lett.*, vol. 4, no. 4, pp. 3750–3757, Oct. 2019.

[32] K. Xu, J. Zhao, and X. Zheng, "Configuration comparison among kinematically optimized continuum manipulators for robotic surgeries through a single access port," *Robot.*, vol. 33, no. 10, pp. 2025–2044, Dec. 2015.

[33] Z. Wu, Q. Li, J. Zhao, J. Gao, and K. Xu, "Design of a modular continuum-articulated laparoscopic robotic tool with decoupled kinematics," *IEEE Robot. Autom. Lett.*, vol. 4, no. 4, pp. 3545–3552, Oct. 2019.

Yuyang Chen received the B.S. degree in mechanical engineering from the School of Mechanical Engineering, Zhejiang University, Hangzhou, China, in 2015. He is currently working toward the Ph.D. degree in mechanical engineering with the UM–SJTU Joint Institute, Shanghai Jiao Tong University, Shanghai, China.

His research interests include surgical robotics and continuum mechanisms.

Chao Zhang received the B.S. and M.S. degrees in clinical medicine from Shanghai Jiao Tong University, Shanghai, China, and the Ph.D. degree from the Second Military Medical University, Shanghai, China. He is currently an Associate Chief Physician with the Urology Department, Changhai Hospital, Second Military Medical University, Shanghai, China. He was selected into the Shanghai Young Physician Training Funding Program in 2015. His research interests include urological oncology and minimally invasive surgery.

Zhonghao Wu (Student Member, IEEE) received the B.S. degree from the School of Mechanical Engineering, Dalian University of Technology, Dalian, China, in 2016. He is currently working toward the Ph.D. degree in mechanical engineering with the UM–SJTU Joint Institute, Shanghai Jiao Tong University, Shanghai, China.

His research interests include surgical robotics and continuum mechanisms.

Jiangran Zhao received the B.S. and Ph.D. degrees in mechanical engineering from the UM–SJTU Joint Institute, Shanghai Jiao Tong University, Shanghai, China, in 2011 and 2017, respectively.

He is currently a Research Scientist with the Beijing Surgerii Technology Company, Ltd., Beijing, China.

Bo Yang received the B.S. and M.S. degrees in clinical medicine from the Second Military Medical University, Shanghai, China, in 1999 and 2001, respectively.

He was a visiting scholar in Cleveland Clinic in 2010. He is currently an Associate Chief Physician with Changhai Hospital, Second Military Medical University, Shanghai, China. His research interests include minimally invasive surgery for renal and prostatic cancers.

Jia Huang is currently working toward the Doctoral degree in clinical medicine with Shanghai Lung Tumor Clinical Medical Center, Shanghai Chest Hospital, Shanghai Jiao Tong University, Shanghai, China.

His current research interest includes robotic-assisted minimally invasive thoracic surgery.

Qingquan Luo received the B.S. degree in clinical medicine from West China Medical Center, Sichuan University, Chengdu, China.

He is currently a Chief Physician with Shanghai Lung Tumor Clinical Medical Center, Shanghai Chest Hospital, Shanghai Jiao Tong University, Shanghai, China.

Dr. Luo is a member of Chinese Medical Association, and a Fellow of the American College of Surgeons. He is specialized and experienced in robotic-assisted minimally invasive thoracic surgery.

Linhui Wang received the B.S. and Ph.D. degrees in clinical medicine from the Second Military Medical University, Shanghai, China, in 1990 and 1999, respectively.

Prof. Wang was the recipient of the National Second Prize for Progress in Sicence and Technology twice. He is currently a Chief Physician in Changhai Hospital. He is also the Director of the Department of Urology and the Director of the Robotic Surgery Center, Changhai Hospital.

Kai Xu (Member, IEEE) received the B.E. and M.S. degrees in mechanical engineering from the Department of Precision Instruments and Mechanology, Tsinghua University, Beijing, China, in 2001 and 2004, respectively, and the Ph.D. (*with distinction*) from the Department of Mechanical Engineering, Columbia University, New York, NY, USA, in 2009.

He is currently a Full Professor with the School of Mechanical Engineering, Shanghai Jiao Tong University, Shanghai, China, and the Director of the Robotics Innovation and Intervention Laboratory. His research interests include surgical robots, prosthetic hands, flexible manipulators, special industrial robots, and continuum mechanisms.